Dielectric dispersion and vibrational studies of a new ferroelectric, glycinium phosphite crystal

1996 J. Phys.: Condens. Matter 8 10647

(http://iopscience.iop.org/0953-8984/8/49/049)

J. Phys.: Condens. Matter **8** (1996) 10647–10658. Printed in the UK

Dielectric dispersion and vibrational studies of a new ferroelectric, glycinium phosphite crystal

J Baran†, G Bator‡, R Jakubas‡ and M Śledź†

† Institute of Low Temperature and Structure Research, Polish Academy of Sciences, Okólna 2, 50-950 Wrocław 2, PO Box 937, Poland

‡ Faculty of Chemistry, University of Wrocław, 50-383 Wrocław, Joliot Curie 14, Poland

Received 16 July 1996

Abstract. The dielectric dispersion in glycine phosphite crystal over the frequency range 30–1000 MHz is presented. Ferroelectric dispersion of the Debye type along the *b*-axis occurs in the microwave-frequency region and is caused by a single relaxational soft mode. The powder IR (at low temperatures between 300 and 14 K) and FT Raman spectra in the region between 4000 and 80 cm^{-1} are measured. DSC measurements for the GPI and deuterated crystals are performed. The results confirm the order–disorder nature of a proper ferroelectric phase transition of second order.

1. Introduction

Glycinium phosphite crystals ($(NH_3CH_2COOH)\cdot H_2PO_3$ abbreviated as GPI) undergo a continuous-type ferroelectric phase transition at 224 K [1]. GPI is thus another ferroelectric crystal of phosphorous acid with an amino acid, like betainium phosphite crystal (abbreviated as BPI) [2]. Above room temperature, the BPI crystal undergoes a ferroelastic–paraelastic phase transition at $T_{c1} = 355$ K [2], which is not present in the case of GPI. Both of these crystals belong to the monoclinic system and they have similar space groups ($P2_1/a$ and $P2_1/c$, respectively, for GPI and BPI). Their structures are built up of the infinite chains of phosphite anions to which the amino acid cations are attached by strong hydrogen bonds [3, 4]. The temperatures of the ferroelectric phase transitions and values of the spontaneous polarizations (1.7×10^{-2} and 5×10^{-2} C m^{-2} for BPI and GPI, respectively) are similar. The spontaneous polarizations are parallel to the monoclinic *b*-axes in both crystals. The isotopic effect (upon deuteration) on the ferroelectric T_c is very large ($T_{cD}/T_{cH} = 1.43$) for the BPI crystal [5] and, as will be shown by the DSC method in this paper, it appears to be similar (1.42) for the GPI crystal. However, there is an important structural difference between these two crystals; i.e. the phosphite chains are parallel to the ferroelectric axis (*b*) in the structure of BPI and perpendicular to it (i.e. parallel to the *c*-axis) in the case of GPI (see figure 1). In both crystals the interphosphite hydrogen bonds are centrosymmetric and they are slightly shorter in the BPI (2.479 and 2.502 Å) than in the GPI (2.482(1) and 2.518(1) Å). The hydrogen bonds between the carboxylic groups and phosphite anions appear to be shorter in the case of BPI (2.493 Å) than in the case of GPI (2.598(1) Å). Although there has been a lot of interest in the investigation of the BPI crystal, the molecular mechanism of its ferroelectric phase transition is not clear yet. It is suggested that besides the ordering of the protons in the interphosphite hydrogen bonds, other molecular motions must also contribute to the ferroelectric phase transition mechanism [6, 7].

0953-8984/96/4910647+12$19.50

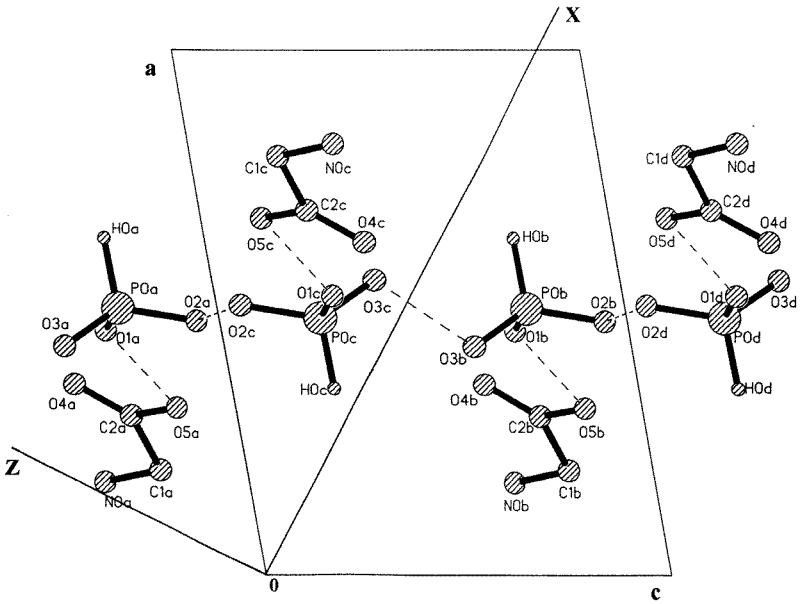

Figure 1. The projection of the structure of the GPI crystal along the monoclinic *b*-axis. The experimental coordinate system $XY(b)Z$ with respect to the crystallographic directions $a, b(Y)$ and c is shown.

The polarized IR and Raman spectra of the BPI single-crystal samples revealed the largest changes of the bands arising from the stretching motions of the phosphite anions [8]. These changes are explained either by a strong coupling between the stretching P–O motions and hydrogen bonds (stretching and bending motions) or by the disorder of the protons in the hydrogen bonds. Recently, polarized reflected IR and Raman spectra of BPI crystal in the low-frequency region were published by Ebert *et al* [9] whose conclusions are not quite consistent with previously published infrared reflection results obtained by Koch and Happ [6].

To get more information about the microscopic nature of the ferroelectric phase transition in GPI crystal, dielectric dispersion studies in the vicinity of the para–ferroelectric phase transition over a wide frequency range between 30 MHz and 1 GHz are performed in this paper. The results are analysed to obtain the critical properties of the relaxation parameters.

Additionally, the powder infrared and FT Raman spectra at room temperature are measured for the GPI crystal and its deuterated analogue (DGPI). The IR spectra for the GPI crystal were also measured at low temperatures (14–300 K). The results of the DSC measurements for normal and deuterated crystals are also presented for the first time.

2. Experimental procedure

The GPI crystals were grown from aqueous solutions containing glycine and phophorous acid in the ratio 1:1. The deuterated crystals were obtained by fourfold crystallization from the D_2O. The single crystals were oriented by applying polarized microscope and x-ray methods. The $XY(b)Z$ orthogonal coordinate system was chosen. The angles $\widehat{Xa}$ and $\widehat{aZ}$ are equal to 37° and 53°, respectively (see figure 1). The X- and Z-directions correspond

to the principal directions of the optical indicatrix for the visible light.

For the dielectric measurements, samples of dimensions $5 \times 5 \times 1$ mm^3 were cut perpendicular to the $Y(b)$-direction. The plates were silver painted. The complex electric permittivity, $\varepsilon^* = \varepsilon' - \mathrm{i}\varepsilon''$, of the GPI crystals was measured by means of a HP 4191A RF Impedance Analyser in the frequency range 30–1000 MHz. The measurements were performed in the temperature range 210–300 K. The temperature was stabilized and controlled by a UNIPAN Temperature Controller Type 650 with fluctuation less than ± 0.1 K. The overall error for the real part of the complex electric permittivity, ε'_b, was less than 5%. The overall error for the imaginary part of the complex electric permittivity, ε'', was less than 7%.

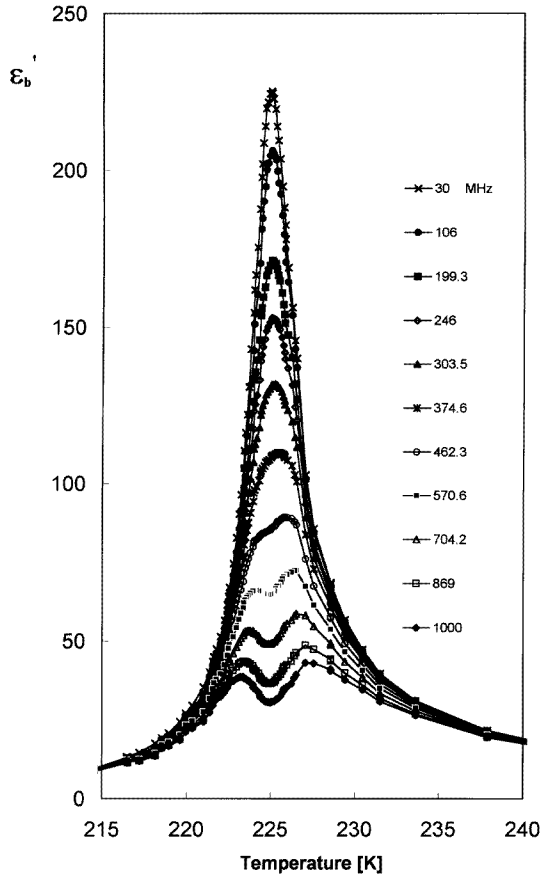

Figure 2. The temperature dependence of the real part of the complex electric permittivity, ε'_b, in the vicinity of $T_c = 225$ K for several frequencies along the b-axis for GPI.

The infrared spectra were measured for the mulls in Nujol and Fluorolube with a Bruker IFS-88 spectrometer, resolution 2 cm^{-1}. The low-temperature (300–14 K) IR spectra were measured only for the sample in Nujol mulls by using a closed-cycle helium cryostat (Displex Closed Cycle Cryogenics Refrigeration System Model CSW-202 and Lakeshore Model 330-11 Dual Sensor Temperature Controller). The Raman spectra were taken with the FT Raman FRA-106 attachment to the Bruker IFS-88 spectrometer using an Nd:YAG

laser pumped by a diode laser; power $\simeq$180 mW, resolution 2 cm^{-1}.

The DSC measurements were performed with a Perkin–Elmer DSC-7 instrument equipped with a CCA-7 low-temperature accessory. The scanning rate was 10 deg min^{-1}. for a temperature range between 100–440 K.

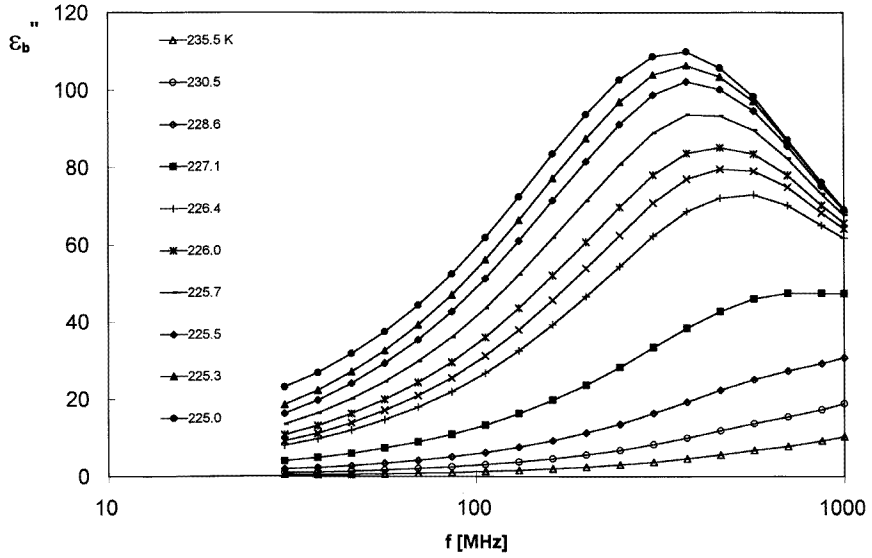

Figure 3. The frequency dependence of the imaginary part of $\varepsilon^*, \varepsilon_b''$, for some temperatures near T_c for GPI.

3. Dielectric dispersion of the GPI crystal

Figure 2 shows the temperature dependence of the real part of the complex electric permittivity ε_b' in the vicinity of $T_c = 225$ K for several frequencies between 30 MHz and 1000 MHz measured along the *b*-axis. The real part, ε_b', shows a peak at 225 K up to 400 MHz and above this frequency it splits into two peaks, the width of which broadens with increasing frequency. The T_c-value obtained for GPI in the present study (225 K) is comparable to that ($T_c = 224$ K) reported previously in [1]. The frequency dependence of the imaginary part ε'' for some temperatures within the paraelectric phase near the temperature T_c is shown in figure 3.

The Cole–Cole plots of the observed relaxation are presented in figure 4. The dielectric relaxation in the GPI crystals is well described by the Cole–Cole relation:

$$\varepsilon^* = \varepsilon_\infty + (\varepsilon_0 - \varepsilon_\infty)/[1 + (\mathrm{i}\omega\tau)^{1-\alpha}] \tag{1}$$

where ε_0 and ε_∞ are the low-frequency and high-frequency limits of the electric permittivity, respectively, and ω is the angular frequency, τ is the relaxation time, and α is the distribution of relaxation times parameter. $\varepsilon_0, \varepsilon_\infty, \tau$ and α are the fit parameters for each temperature independently. The small values of α ($\alpha < 0.02$) indicate the almost monodispersive nature of the dielectric relaxation in GPI. The α-parameter is independent of temperature even in the vicinity of T_c.

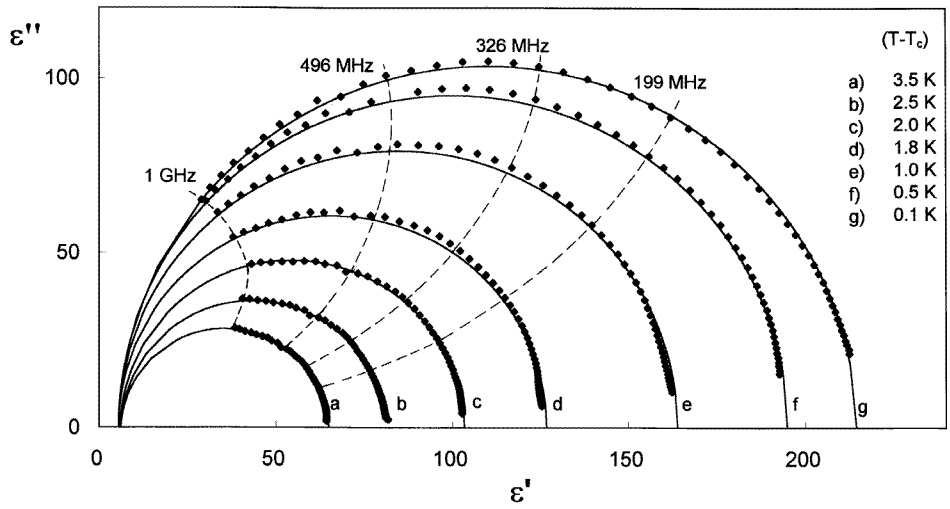

Figure 4. A Cole–Cole diagram for GPI in the paraelectric phase.

The results presented in figures 2–4 indicate that the fundamental ferroelectric dispersion appears in the microwave-frequency region . The relaxational-soft-mode dynamics reveals itself in the frequency region characteristic for the H-bonded ferroelectrics [10]. On approaching the Curie temperature, the macroscopic relaxation time reaches the value $\tau = 4 \times 10^{-10}$ s. This value is comparable with that of other hydrogen-bonded ferroelectrics like TGS-family crystals [11], CsH_2PO_4 [12] and RbD_2PO_4 [13].

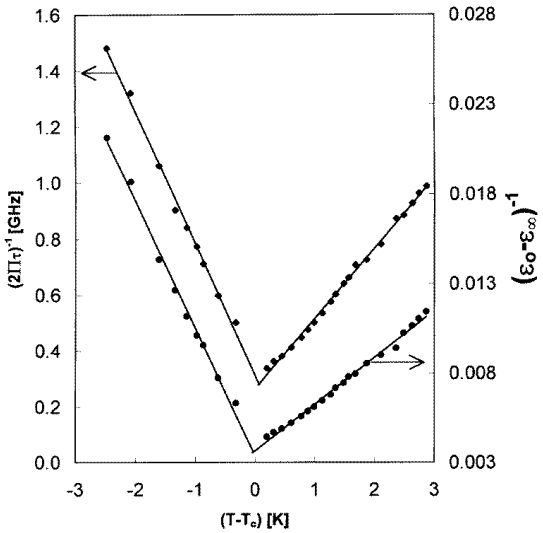

Figure 5. The temperature dependence of the soft-relaxational-mode frequency $\nu_s = (2\pi\tau)^{-1}$ (upper data) and the inverse dielectric increment $(\varepsilon_0 - \varepsilon_\infty)^{-1}$ (lower data) for GPI.

The temperature dependence of the soft-relaxational-mode frequency $\nu_s = (2\pi\tau)^{-1}$ and the inverse dielectric increment $(\varepsilon_0 - \varepsilon_\infty)^{-1}$ are shown in figure 5. The relaxation

frequency in the paraelectric phase varies according to the law $\nu_s = 251(T - T_0)$ MHz, where $T_0 = 224$ K, and causes the Curie–Weiss behaviour of $\varepsilon_0 - \varepsilon_\infty$ with the Curie–Weiss constant $C_p = 383$ K. The ratio of the Curie constants ($C_p/C_f = 383/141 = 2.7$, where C_f is the Curie–Weiss constant estimated in the ferroelectric phase) is typical of the ordinary second-order phase transition.

The activation free energy $\Delta F^{\#}$ was calculated according to the Eyring equation:

$$\tau_0 = (h/kT)\exp(\Delta F^{\#}/kT) \tag{2}$$

where the microscopic relaxation time τ_0 is related to the macroscopic one, τ, according to the following formula [14]:

$$\tau_0 = \varepsilon_\infty/(\varepsilon_0 - \varepsilon_\infty)\tau. \tag{3}$$

The value of $\Delta F^{\#} = 17$ kJ mol^{-1} is relatively high and is typical for crystals containing large-size organic cations contributing to the mechanism of the phase transition.

The above-presented results on the dielectric response are characteristic of a para–ferroelectric phase transition of second-order type, where a critical slowing down of the ferroelectric order parameter fluctuations is observed. The relaxational mode softens to 250 MHz at T_c.

4. Infrared and Raman spectra

The powder IR and Raman spectra of the GPI and its deuterated analogue (DGPI) at room temperature are shown in figure 6. The wavenumbers of the bands are listed in table 1. The powder IR spectra of the GPI at low temperatures are presented in figure 7. The infrared spectrum of the GPI is characterized by a broad background which extends over the region between $\simeq$3200 and 1200 cm^{-1}. The high-wavenumber part of that absorption arises from the stretching vibrations of the $-NH_3^+$ groups. The stretching vibrations (3021 and 2986 cm^{-1}) of the CH_2 groups are superimposed on it. The strong band at 2921 cm^{-1} arises from the stretching vibration of the longest (O(5)–H...O(1)) hydrogen bond. The bands in the region between 2900–2500 cm^{-1} are also due to that mode; however, some of them may arise from the overtones of the deformation vibrations of the $-NH_3^+$ groups. The remaining part of the broad absorption must be assigned to the stretching vibrations of the interphosphite hydrogen bonds (O(2a)...O(2c) and O(3c)...O(3b)) which are very strong (the O...O distances are equal to 2.482 and 2.518 Å, respectively) and centrosymmetric with disordered protons in the paraelectric phase. However, at present it is quite difficult to say anything more about their absorption in the IR spectrum. The sharp band at 2419 cm^{-1} observed in both IR and Raman spectra arises from the stretching vibrations of the PH bond. Its wavenumber is characteristic for the $H_2PO_3^{1-}$ anion [15, 16] and it is higher than that (2380 cm^{-1}) in the spectra of the BPI crystal [8, 9]. One band observed for the νPH clearly proves that only one type of phosphite anion is present in both phases. The glycine molecules appear in the form of the glycinium cations $NH_3^+CH_2COOH$. The most characteristic stretching mode (νCO) of the C=O bond appears at 1727 cm^{-1} and 1723 cm^{-1} in IR and Raman spectra, respectively [17]. The band at 1750 cm^{-1} in the IR and Raman spectra arises from the overtone of the stretching C–C bond (875 cm^{-1}) vibration being so strong due to the Fermi resonance [17]. Accidentally, it coincides with the stretching νPD mode (1754 cm^{-1}) for the deuterated sample. The νC=O band shifts to 1716 cm^{-1} on deuteration. This indicates some coupling between that mode and the proton vibrations (of the hydrogen bonds and/or NH_3^+ groups). The bands in the region between 1150 and 900 cm^{-1} arise from the stretching vibrations of the PO_3 groups and bending (in-plane and

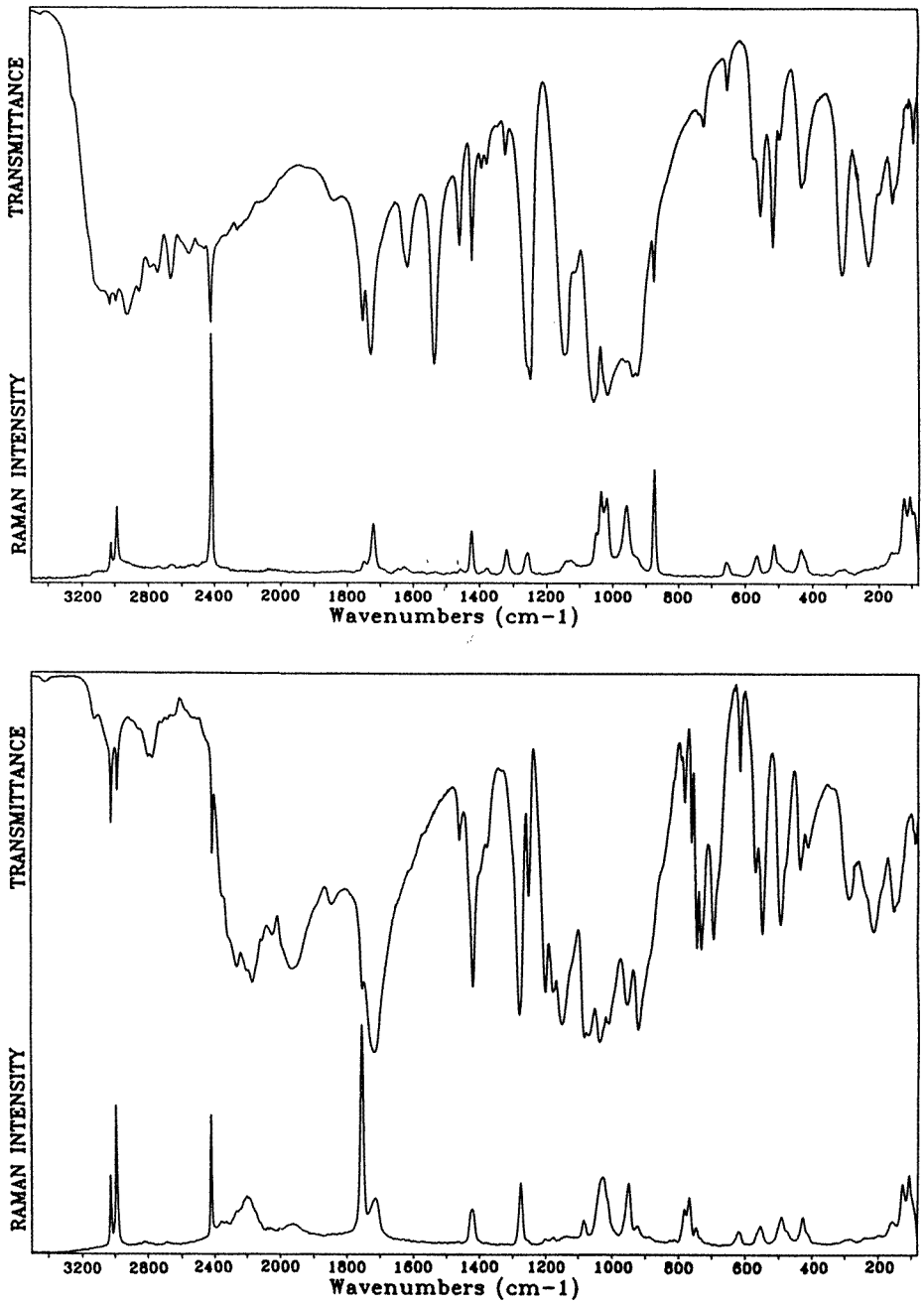

Figure 6. The powder IR and FT Raman spectra of GPI (upper) and DGPI (lower) at room temperature.

out-of-plane) vibrations of the P–H bond. The deformation modes of the PO_3 group of the phosphite ions appear in the region between 600 and 400 cm^{-1}, where also the bands of the deformation (wagging and rocking) modes of the COOH group appear. More precise

Table 1. The wavenumbers (cm^{-1}) and relative intensities observed in the powder infrared and FT Raman spectra of the glycinium phosphite (GPI) and its deuterated analogue (DGPI) measured at room temperature. Abbreviations: vs—very strong; s—strong; m—medium; w—weak; vw—very weak; sh—shoulder; b—broad.

GPI Infrared	GPI FT Raman	DGPI Infrared	DGPI FT Raman	GPI Infrared	GPI FT Raman	DGPI Infrared	DGPI FT Raman
3442vw		3420vw		1457m	1459vw	1460m	
3250wsh				1419m	1424m	1417vs	1421w
3126ssh		3124vw		1390w		1397msh	
3100ssh	3100vwb			1374w	1378vw	1376m	
3024s	3023w	3021m	3026m	1344vw		1335wsh	
2986s	2988m	2986w	2987s	1319w	1321w		
2921s						1278vs	1285m
2847s		2862vwsh		1259vssh	1261w		
			2817vwb	1250vs		1252m	1254vwsh
2781m		2802w				1200vs	1199vw
2736m	2738vwb	2779w				1176vs	1175vw
		2722vw		1144vs	1141wsh	1147vs	1138vwb
		2690vw	2685vwb		1127w		
2657m	2657vwb	2650vw		1111m		1116ssh	
		2582vwsh				1079vs	1081w
2548m	2540vwb	2542vw				1066vs	
		2512vw		1058vs			
2485m	2470vwb			1048vssh	1049msh		
2455m		2455vwsh		1027vssh	1036m		
2418s	2419vs	2419m	2420s			1033vs	
		2357msh	2357wb			1021vssh	1025m
2320msh	2318vwb	2320ssh	2327wb	1015vs	1018m		
		2266s	2262wsh			1010vssh	1011msh
2252m		2205s	2200wb			1005vs	
2195msh		2171s	2185wsh	961vs	959m	951vs	948m
		2115s		938vs	930wsh		
2100mb	2070vwb	2051s	2060vwb	925vs			
		1966s	1966wb				923w
1923msh		1890msh				918vs	
1836m		1845m		874s	875s	884ssh	888vw
		1753vs	1754vs	850sh		848msh	
1751s	1750w					811wsh	
1727vs	1723m	1716vs	1715m			791vw	
1626msh	1648vw					780w	780m
1615m	1628vw	1608msh				760m	766m
	1571vwb					743s	746w
1535vs	1532vwb						

assignment of the bands will be given in our next paper, which will report the results on the polarized Raman and infrared spectra of the single-crystal samples. At present attention will be concentrated on the changes observed in the IR spectra of GPI measured at low temperatures. The changes in the spectra measured close to the ferroelectric phase transition, respectively at 240 and 190 K, are quite small (see figure 7). The splittings are observed for the bands arising from the stretching vibration of the C=O bond, rocking vibrations of the CH_2 group ($\simeq$1319 cm^{-1}) and the COOH bending (652 cm^{-1}) vibration. Additionally, new bands appear at 1099 cm^{-1}, 481 cm^{-1}, 452 cm^{-1} and 252 cm^{-1}. Much greater changes occur in the spectra taken at 14 K. Especially great ones are observed for the asymmetric

Table 1. (Continued)

GPI Infrared	GPI FT Raman	DGPI Infrared	DGPI FT Raman
		729s	732vwsh
		691s	
		678msh	
652vw	656w		
		630vw	
		614w	617w
574w	564w	567m	566wsh
554m		545s	554w
517m	514w		
495w	495vwsh	491s	490w
		477msh	475wsh
432w	433w	433m	426w
422wsh	420wsh		
		409m	412wsh
		338vwsh	
	320vwsh		
311m			
	305vw		
			296vwsh
		283m	280vw
		235msh	
227m			
		210m	
195wsh			198vw
	163w		
154w	150w	149m	157w
144wsh		143msh	
137wsh		138wsh	
124vwsh	125m	124wsh	126m
107vw	109m		106m
93w	96m	93wsh	
		88w	

bending vibrations of the NH_3^+ group (at $\simeq$1630 cm^{-1}) and for the stretching (the region between 1100 and 900 cm^{-1}) and deformation vibrations ($\simeq$600–400 cm^{-1}) of the phosphite ions. This may suggest that other phase transitions occur at temperatures lower than 100 K. The changes involved in the ferroelectric phase transition seem to indicate an order–disorder type of phase transition. Very likely two crystallographically different glycinium cations appear in the ferroelectric phase. Taking into account the lack of any significant changes of the bands arising from the internal vibrations of the phosphite ions, one may suggest that the phosphite anions remain very similar in the ferroelectric and paraelectric phases at temperatures close to T_c.

5. The DSC results

The DSC diagrams of the GPI and DGPI samples for the cooling-down and heating-up runs are shown in figure 8. The observed anomalies at 225 K and at $\simeq$315 K for GPI and DGPI, respectively, clearly indicate second-order phase transitions. The temperatures of the phase

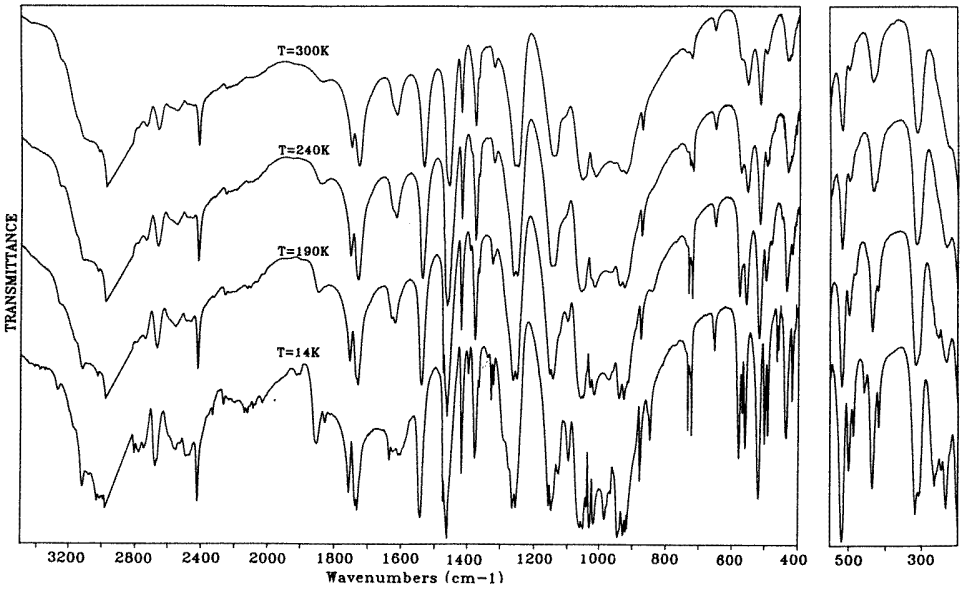

Figure 7. The powder IR spectra of GPI (in Nujol mulls) measured between 300 and 14 K.

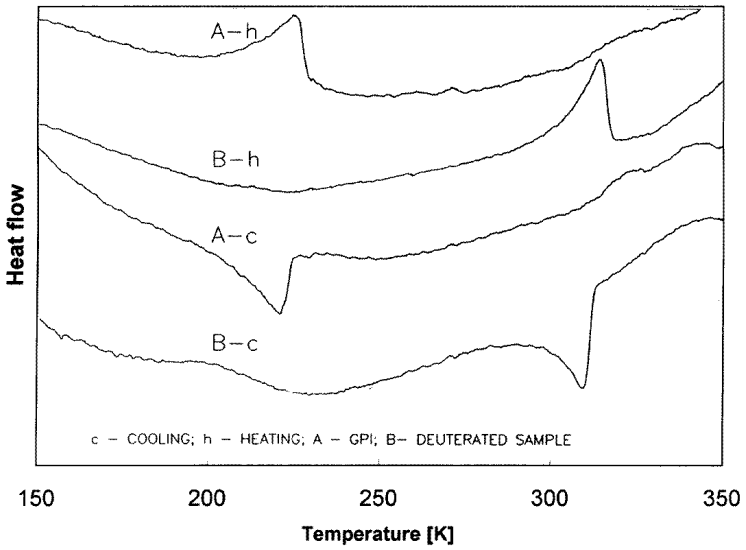

Figure 8. DSC diagrams for GPI and its deuterated analogue, DGPI, measured for cooling and heating runs.

transitions for the deuterated crystal strongly depend on the sample preparation. This is due to the fast replacement of deuterium by protons from moisture. The replacement is faster for a well ground sample. For a gently ground sample the phase transition temperature was determined as 323 K. These results clearly prove that the paraelectric–ferroelectric phase transition is shifted by 98 K for maximal deuteration; i.e. for the sample of the chemical

formula $(ND_3CH_2COOD)\cdot D_2PO_3$. Our primary dielectric measurements show that the phase transition is also of ferroelectric–paraelectric type for the deuterated sample. Full results of our dielectric measurements for the deuterated sample will be published in a separate paper. Except the paraelectric–ferroelectric transition no other phase transition is detected by the DSC method. The crystal is stable till $\simeq$423 K is reached where the decomposition of the sample begins.

6. Discussion

The missing information on the crystal structure in the ferroelectric phase prevents us from discussing the accurate mechanism of the paraelectric–ferroelectric phase transition. A very large isotopic effect ($\simeq$98 K) on T_c indicates the essential role of the interphosphite hydrogen bonds in the phase transition mechanism. According to the x-ray crystal data these hydrogen bonds are centrosymmetric with disordered protons [4]. The infrared and Raman spectra show that the normal $H_2PO_3^{1-}$ anions appear in the paraelectric and ferroelectric phase. This confirms that the protons in these hydrogen bonds do not occupy the centre of the interphosphite hydrogen bonds, but they are dynamically disordered in such a way that on the time-scale of the vibrational spectroscopy one can see dihydrogen phosphite anions. Very likely the dynamical disorder of these protons is coupled to the motions of the glycinium cations. Therefore, only one type of glycinium cation is observed by the vibrational methods in the paraelectric phase. In the ferroelectric phase the splittings of some glycinium bands are observed. This may indicate that two different glycinium cations appear in the ferroelectric phase. Thus, the spontaneous polarization appears due to the ordering of the glycinium cations which also force protons into ordering. This seems to be in accordance with the dielectric measurement. To throw more light on the mechanism of the paraelectric–ferroelectric phase transition, it is necessary to compare the dielectric dispersion results obtained for two similar crystals: BPI and GPI. The investigation of the critical dielectric relaxation [7] indicates that the ferroelectric dynamics of the BPI crystal is described in terms of the soft relaxational mode associated with the proton flipping motion in the double potential well with the activation energy $\Delta E = 5$ kJ mol^{-1} in the paraelectric phase. In a case of the GPI crystal the macroscopic relaxation time ($\tau = 4 \times 10^{-10}$ s at T close to the T_c) is nearly one order of magnitude longer in comparison to that ($\tau = 6.6 \times 10^{-11}$ s) found for BPI [6]. The activation energy (ΔE) estimated from this measurement is more than three times higher than that obtained for BPI. This implies that the mechanism of the para–ferroelectric phase transition in GPI crystals seems not to be strictly connected with only movements of the protons in the strong hydrogen bonds. Therefore it might be suggested that the dynamics of the organic sublattice (glycinium cations) could play a key role in the long-range order.

However, one should remember that the role of hydrogen bonds in GPI was clearly demonstrated by the distinct deuteration effect on T_c. In our opinion the mechanism of the phase transition at 225 K in GPI is rather more complex than in a typical ferroelectric [18].

It is worth mentioning that the space group $P2_1$ is clearly indicated by the recently performed x-ray investigation of deuterated GPI in the ferroelectric phase (at room temperature) [18]. The same space group is expected for the normal GPI crystal. Therefore, the para–ferroelectric phase transition is $P2_1/a \rightarrow P2_1$. Such a sequence of the phase transition is consistent with the previous measurements of the spontaneous polarization which was observed only along the *b*-axis [1].

Acknowledgment

This work was supported by KBN project register No 2P 303 110 06.

References

[1] Dacko S, Czapla Z, Baran J and Drozd M 1996 *Phys. Lett.* at press
[2] Albers J, Klöpperpieper A, Rother H J and Haussühl S 1988 *Ferroelectrics* **81** 27
[3] Fehst I, Paasch M, Hutton S L, Braune M, Brohmer R, Loidl A, Dorffer R, Narz T T, Haussühl S and McIntyre G J 1993 *Ferroelectrics* **138** 1
[4] Averbuch-Pouchot M T 1993 *Acta Crystallogr.* C **49** 815
[5] Launer S, Maire M L, Schaack G and Haussühl S 1992 *Ferroelectrics* **132** 257
[6] Koch G and Happ H 1993 *Ann. Phys. Lpz.* **2** 522
[7] Sobiestianskas R, Grigas J, Czapla Z and Dacko S 1993 *Phys. Status Solidi* a **136** 223
[8] Baran J, Czapla Z, Drozd M, Ilczyszyn M M, Marchewka M and Ratajczak H 1996 *J. Mol. Struct.* at press
[9] Ebert H, Lanceros-Mendez S, Schaak G and Klöpperpieper A 1995 *J. Phys.: Condens. Matter* **7** 9305
[10] Mizeris R, Grigas J, Levitsky R R, Zachek I R and Sorokov S I 1990 *Ferroelectrics* **108** 261
[11] Takayama K, Deguchi K and Nakamura E 1984 *J. Phys. Soc. Japan* **53** 4121
[12] Kanda E, Tamaki A and Fujimura T 1982 *J. Phys. C: Solid State Phys.* **15** 3401
[13] Komukae M and Makita Y 1985 *J. Phys. Soc. Japan* **4** 4359
[14] Muser H E and Unruh H G 1966 *Z. Naturf.* a **21** 783
[15] Bickley R I, Edwards H G M, Knowles A, Tait J K F, Gustar R E, Mihara D and Rose S J 1994 *Spectrochim. Acta* A **50** 1277
[16] Barnoyer B, Brun G and Maurin M 1970 *Revue Chim. Minerale* **7** 941
[17] Khanna R K, Horak M and Lippincott E R 1966 *Spectrochim. Acta* **22** 1759
[18] Pietraszko A, Damm J, Baran J and Śledź M 1996 unpublished results